

Article

Matere Bonds in Technetium Compounds: CSD Survey and Theoretical Considerations

Sergi Burguera , Rosa M. Gomila , Antonio Bauzá  and Antonio Frontera *Department of Chemistry, Universitat de les Illes Balears, Crta. de Valldemossa km 7.5,
07122 Palma de Mallorca, Spain

* Correspondence: toni.frontera@uib.es

Abstract: Noncovalent interactions involving metals as electron acceptors are continuously under investigation. The term “matere bond” has been proposed to identify noncovalent donor–acceptor interactions where elements of group 7 of the periodic table play the role of the electrophilic site. Most of the works on matere bonds involve rhenium atoms usually in +7 oxidation state. This work emphasizes for the first time their importance in technetium derivatives in several oxidation states (+7, +6, +5, and +3). The Cambridge Structural Database (CSD) in combination with density functional theory (DFT) calculations are used to demonstrate the structure directing role of matere bonds in X-ray structures, even involving anion–anion interactions. Further characterization of the matere bonds is provided using Molecular Electrostatic Potential (MEP) surface calculations, the “Quantum Theory of Atoms in Molecules” (QTAIM), and Natural Bond Orbital (NBO) analyses. It should be emphasized that some types of matere bonds reported herein have not been previously described in literature.

Keywords: noncovalent interactions; matere bonds; technetium; CSD survey; DFT calculations



Citation: Burguera, S.; Gomila, R.M.; Bauzá, A.; Frontera, A. Matere Bonds in Technetium Compounds: CSD Survey and Theoretical Considerations. *Crystals* **2023**, *13*, 187. <https://doi.org/10.3390/cryst13020187>

Academic Editor:
Sławomir Grabowski

Received: 29 December 2022
Revised: 16 January 2023
Accepted: 17 January 2023
Published: 20 January 2023

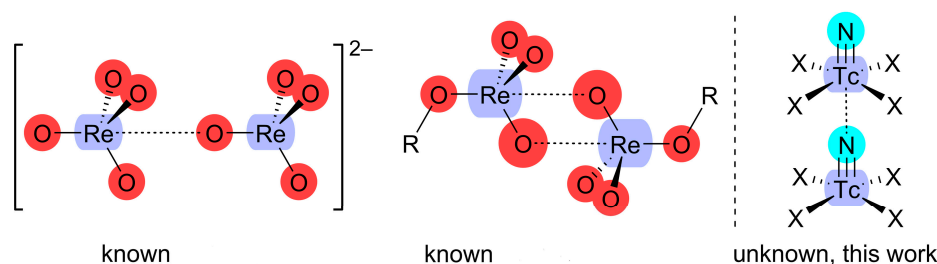


Copyright: © 2023 by the authors. Licensee MDPI, Basel, Switzerland. This article is an open access article distributed under the terms and conditions of the Creative Commons Attribution (CC BY) license (<https://creativecommons.org/licenses/by/4.0/>).

1. Introduction

Noncovalent interactions involving metals are object of continuous investigation, including the differentiation between coordination bonds and σ -hole interactions [1–3]. The most studied interactions are spodium [4–6] and regium (or coinage) bonds [7–9], where post-transition metals of groups 12 and 11, respectively, play the role of Lewis acid. This type of interactions is fruit of the expansion of the σ -hole concept developed to explain the interactions of elements of the p-block to the transition and post transition elements [7]. Apart from the terms spodium and regium bonds, other names have been proposed for elements of group 8 (osme bonds) [10], group 7 (matere bonds) [11], and group 6 (wolfium bonds) [12]. In general, X-ray structures where osme, matere, or wolfium bonds are relevant to understand their solid-state packing involve the heavier elements of the groups (tungsten, rhenium, and osmium) [10–12]. In the particular case of matere bonds, they have been described in perrhenate anion–anion interactions [11], methyltrioxorhenium (VII) [13], and perrhenate esters (see Scheme 1) [14], however they have not been analyzed in depth in technetium derivatives, especially in oxidation states +6, +5, and +3.

In this manuscript, the ability of Tc to form matere bonds is evidenced by exploring the Cambridge structural database (CSD) [15] and rationalized by means of density functional calculations. In particular, eight X-ray structures retrieved from the CSD were selected to illustrate the importance of matere bonds in the solid state. DFT calculations were used to demonstrate the attractive nature of the interaction, combined with molecular electrostatic potential (MEP) surfaces to evidence the existence of a σ -hole at the Tc-atom and the directionality of the matere bond. Furthermore, the noncovalent nature of the interaction has been confirmed using the quantum theory of atoms in molecules (QTAIM) and the noncovalent interaction (NCI) plot methods. Finally, charge transfer effects have been studied using the natural bond orbital (NBO) analysis.



Scheme 1. Left: reported matere bonds in perrhenate derivatives. Right: an example of the matere bonds reported herein [11,14].

2. Methods

The CSD version 5.42 (update September 2022) [15] was manually inspected to select the X-ray structures described in this work. Dimers, trimers, and tetramers extracted from the X-ray structures were computed using the Turbomole 7.0 program [16]. Single point calculations have been carried out at the PBE0-D3/def2-TZVP [17–19] level of theory since it has been previously used to study matere bonds [11,13,14]. For two dimers, fully optimizations have been performed in vacuum and in water using the continuum like screening model (COSMO) as implemented in Turbomole 7.0 program [16]. The electrostatic potential surfaces were plotted using the 0.001 a.u. isosurface. The QTAIM [20] and NCIPLOT [21] methods were used to characterize the noncovalent interactions studied herein using the VMD program [22]. Natural Bond Orbital (NBO) [23] calculations were performed using the NBO7.0 program [24]. The NCIPLOT settings used in this work were: RDG = 0.45, density cut-off 0.04 a.u., and color range ± 0.03 for (sign λ_2) ρ . Blue and green are used for attractive interactions and red and yellow for repulsive interactions.

3. Results and Discussion

This section has been divided into four subsections to illustrate four different types of matere bonds found in the CSD search, which are anion...anion, “charge-reverse” anion...cation, anion...Lewis-base, and conventional Lewis acid...Lewis base.

3.1. Anion...Anion Matere Bonds

Matere bonds were initially described in tetroxide anions of group 7 elements as a new case of attractive σ -hole interactions [11]. By combining single crystal X-ray analyses and theoretical calculations, it was demonstrated that in crystalline permanganate and perrhenate salts the metal can act as electron acceptor. That is, the oxygen of an adjacent Mn/ReO₄[−] anion can donate charge and create a supramolecular anionic dimer (or polymeric chains). In this original work, evidence for the existence of matere bonds in X-ray structures of pertechnetate was also provided by analyzing the CSD, however no examples were described or theoretically analyzed. Herein, two structures have been selected from the CSD, which are AMOGIS [25] and AZEMUO [26], where the pertechnetate forms dimers assisted by the protonated amines (counterions).

The solid-state structures of AMOGIS and AZEMUO (see Figure 1) revealed the presence of several N–H...O hydrogen bonds (HBs) connecting the pertechnetate to the cations. Apart from these charge-assisted HBs and the electrostatic cation–anion attraction, linear O–Tc...O contacts are present in both systems. In AMOGIS, one O-atom of TcO₄[−] gets close to technetium of the adjacent anion. The geometry of the contact supports a σ -hole bonding as the O–Tc...O angle is 172.9° and the distance is shorter than the sum of van der Waals radii [$\Sigma R_{\text{vdw}}(\text{Tc} + \text{O}) = 3.60 \text{ \AA}$]. In AZEMUO, two symmetrically equivalent O–Tc...O matere bonds (MaB) form a parallelepiped shaped dimer with a O–Tc...O angle of 168.9° and a distance that is almost identical to $\Sigma R_{\text{vdw}}(\text{Tc} + \text{O})$.

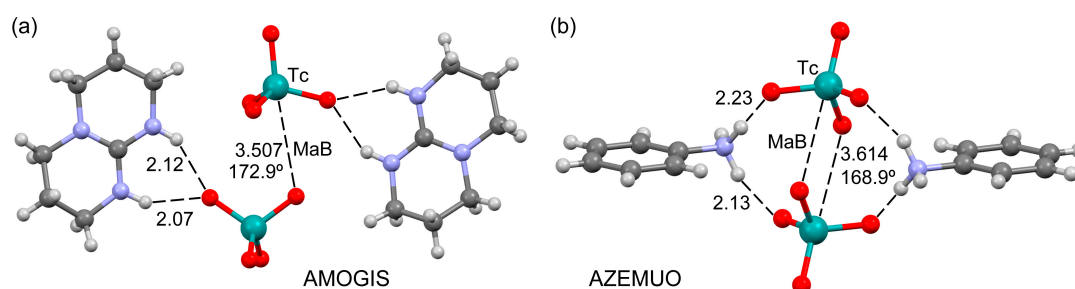


Figure 1. Ball and stick representation of the X-ray structures AMOGIS (a) and AZEMUO (b). Distances in Å. Color code: Carbon grey, Oxygen red, Nitrogen blue, Technetium teal, Hydrogen light grey.

The mature bonds in both systems were analyzed theoretically. Figure 2a shows the MEP surface of the pertechnetate anion. Expectedly, the MEP values of the isolated anion are negative in the entire surface. In more detail, four negative σ -holes are present at the extensions of the four O–Tc bonds. Previous studies have demonstrated that the σ -holes at the pertechnetate anion become positive if the counteraction is considered in the calculation of the MEP [11]. The combined QTAIM/NCIplot analysis of tetrameric assemblies of AMOGIS and AZEMUO are also included in Figure 2b,c. The analysis shows an interesting H-bonding network connecting the anions and cations, combining $\text{NH} \cdots \text{O}$ and $\text{CH} \cdots \text{O}$ interactions. Each hydrogen bond is characterized by a bond critical point (CP, represented as a red sphere) and bond path (orange line) connecting the O and H-atoms. Moreover, the H-bonds are also revealed by the NCIplot analysis, showing blue and green reduced density gradient (RDG) isosurfaces. The mature bonds are not characterized by bond CPs and bond paths connecting the Tc and O-atoms, as previously observed in permanganate. In contrast, the NCIplot analysis revealed the existence of such contacts, showing extended green isosurfaces between the anions. The binding energies of the assemblies are very large in both X-ray structures (-175.7 kcal/mol and -214.3 kcal/mol for AMOGIS and AZEMUO, respectively) due to the ion pair nature of the interaction.

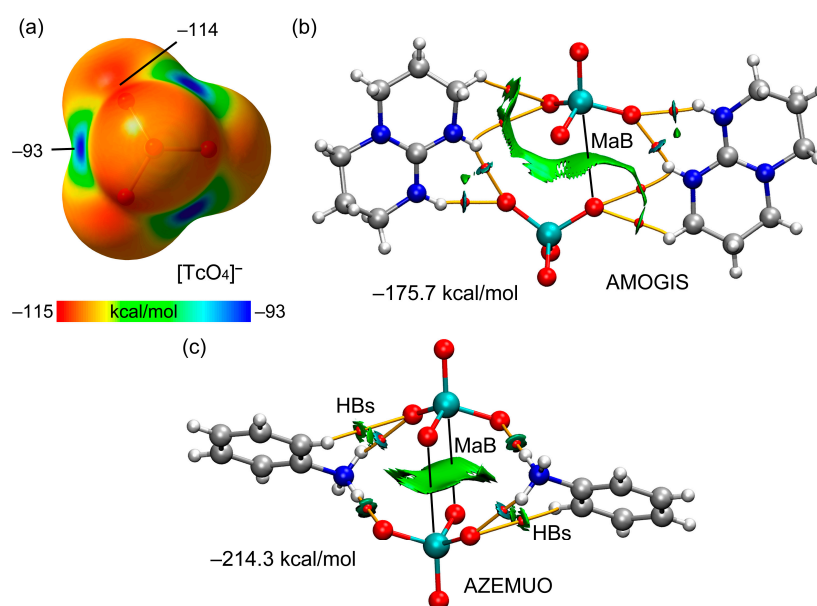


Figure 2. (a) MEP surface of $[\text{TcO}_4]^-$ (isosurface 0.001 a.u.). Energies at selected points in kcal/mol. (b) QTAIM/NCIplot analysis of the tetramers of AMOGIS (b) and AZEMUO (c) with indication of the association energies. Only the bond CPs corresponding to the HBs are shown. Additional bond CPs interconnecting the O-atoms of the anions have been omitted for clarity. Color code: Carbon grey, Oxygen red, Nitrogen blue, Technetium teal, Hydrogen light grey.

An interesting structure is represented in Figure 3 where anion \cdots anion MaBs dictate the formation of an infinite 1D assembly [27]. In this example, the lone pair at the N-atom of one tetrachloro-nitrido-technetate anion points to the Tc-atom of the next $[\text{TcNCl}_4]^-$ anion opposite to the $\text{Tc}\equiv\text{N}$ bond. This 1D assembly is flanked by catena-((μ^2 -18-Crown-6)-cesium) counterions, forming an “infinite sandwich” Cs^+ cation/crown ether. Similar 1D anion \cdots anion assemblies have been recently described and studied theoretically in nitrido-osmium (VI) complexes, presenting similar square-pyramidal geometries [28].

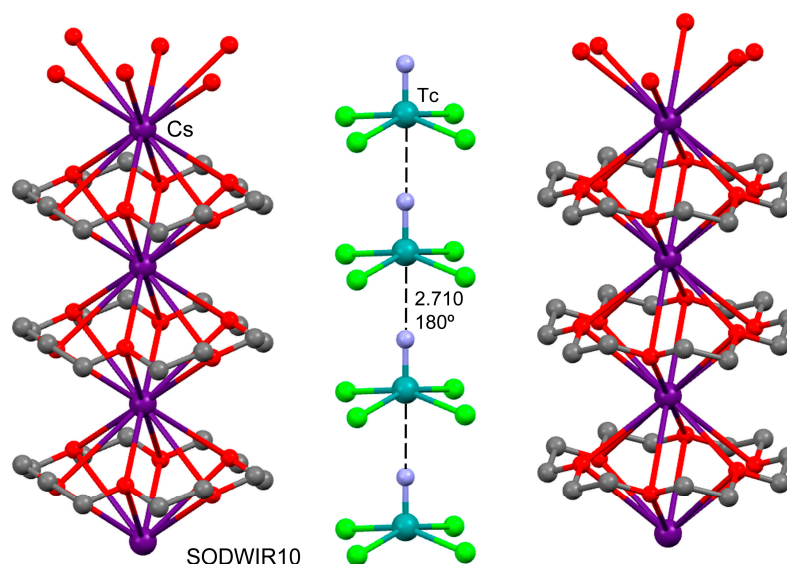


Figure 3. Ball and stick representation of the X-ray structure SODWIR10. Distance in Å. Color code: Carbon grey, Chlorine green, Nitrogen blue, Technetium teal, Cesium purple.

Figure 4a shows the MEP surface of the $[\text{TcNCl}_4]^-$ anion that, as expected, exhibits negative MEP values in the entire surface. However, the existence of a σ -hole opposite to the $\text{Tc}\equiv\text{N}$ bond that corresponds to the MEP maximum (-56 kcal/mol) can be clearly appreciated. The MEP minimum is located between the Cl-atoms at the basal plane and the MEP value at the nitrido N-atom is -71 kcal/mol. The combined QTAIM/NCIplot analysis is given in Figure 4b, evidencing the presence of a bond CP and bond path connecting the Tc atom to the N-atom, thus further supporting the existence of the MaB. It is further characterized by a dark blue RDG isosurface coincident with the location of the bond CP. The blue region is flanked by yellowish regions, indicating some N \cdots Cl repulsion. The NCIplot analysis also discloses the existence of weak Cl \cdots Cl van der Waals interactions. The interaction energy is obviously unfavorable ($+85.4$ kcal/mol) due to the Coulombic repulsion between the counterions, although the Tc \cdots N contact is attractive (blue RDG color).

A differentiating feature of the σ -hole noncovalent interactions in comparison to conventional coordination bond is the existence of an orbital donor–acceptor charge transfer from a lone pair (LP) or π -orbital located at the electron donor and an antibonding σ^* -orbital [29]. A convenient computational tool to analyze such effects is the natural bond orbital (NBO) and the second-order perturbation analysis [23]. The NBO analysis of the anion \cdots anion dimer of SODWIR10 is shown in Figure 4c, confirming the σ -hole nature of the interaction. That is, the filled LP orbital at the sp hybridized N-atom interacts with the antibonding $\sigma^*(\text{Tc}-\text{N})$ with a concomitant stabilization energy of $E^{(2)} = 5.13$ kcal/mol, thus evidencing that the contribution of the MaB interaction is favorable even in the dominant anion \cdots anion repulsion, in line with NCIplot analysis.

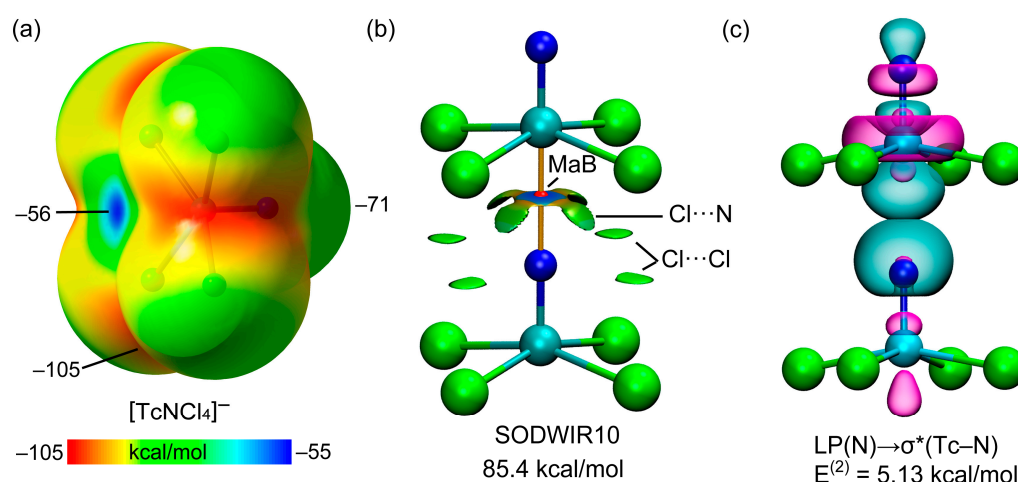


Figure 4. (a) MEP surface of $[\text{TcNCl}_4]^-$ (isosurface 0.001 a.u.). Energies at selected points in kcal/mol. (b) QTAIM/NCIPlot analysis of the dimer of SODWIR10 with indication of the dimerization energy. (c) Plot of the NBOs involved in the donor–acceptor interaction with indication of the $E^{(2)}$ energy. Color code: Chlorine green, Nitrogen blue, Technetium teal.

3.2. Anion ··· Cation Matere Bonds

A remarkable example of an X-ray structure exhibiting cation ··· anion MaBs is given in Figure 5 [30]. This MaB is particularly relevant because it can be understood as a “charge reverse” matere bond in the sense that the electron charge transfer goes from the cation to the anion. That is, the cation is acting as a Lewis base and the anion as a Lewis acid in this particular contact. This compound is a salt formed by *bis*(*N,N*-diethyldithiocarbamato)-gold(III) cation and tetrachloro-nitrido-technetate(VI) anion. As can be observed in Figure 5, two S-atoms of the carbamate ligands are located opposite to the $\text{Tc}\equiv\text{N}$ bonds of two different anionic units, establishing quite directional (178.5°) matere bonds. The $\text{Tc}\cdots\text{S}$ MaB distance is shorter than the sum of the van der Waals radii ($\Sigma R_{\text{vdw}}(\text{Tc} + \text{S}) = 3.85 \text{ \AA}$).

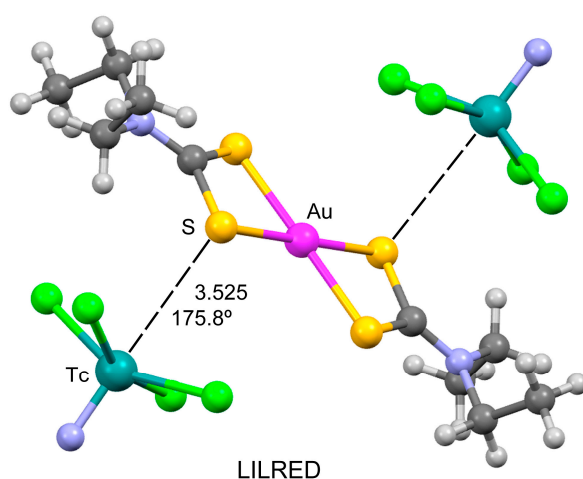


Figure 5. Ball and stick representation of the X-ray structure LILRED. Distance in \AA . Color code: Carbon grey, Chlorine green, Nitrogen blue, Technetium teal, Gold pink, Sulfur yellow, Hydrogen light grey.

Figure 6a shows the MEP surface of the cationic part of the salt (the anionic part is shown in Figure 4a, since it is the same than in SODWIR10). As expected, the MEP surface is positive at all parts of the surface. Remarkably, the MEP minimum is located at the S-atoms over the AuS_4 plane, in good agreement with the geometry of the trimeric assembly shown in Figure 5. Therefore, the MEP minimum of the cation is interacting with the MEP maximum of the anion, which is not the most favored combination from an

electrostatic point of view. This clearly indicates that the MaB in LILRED is influencing the final solid-state geometry even in the presence of strong electrostatic effects. The combined QTAIM/NCIplot analysis of Figure 6b shows the presence of bond CPs and bond paths connecting the Tc atoms to the S-atoms, thus confirming the existence of the MaB. Aside from the MaBs, the anionic units are connected to the cation by additional interactions, including hydrogen bonds, Au \cdots Cl, and Cl \cdots S interactions, as revealed by the distribution of bond CPs and bond paths. These contacts are also revealed by the NCIplot RDG isosurfaces. The interaction energy of the trimer is large and negative (−56.0 kcal/mol) due to the ion-pair nature of the interaction. The NBO analysis of a dimer of LILRED is shown in Figure 6c. That is, a filled LP at the S-atom located in a p-atomic orbital perpendicular to the molecular plane interacts with the antibonding σ^* (Tc–N) with a concomitant stabilization energy of $E^{(2)} = 0.8$ kcal/mol, thus evidencing the σ -hole nature of the interaction. In this case, the orbital contribution is small (compared to SODWIR10 structure) because the Tc \cdots S distance is significantly longer in LILRED, thus diminishing the overlap between the donor and acceptor orbitals.

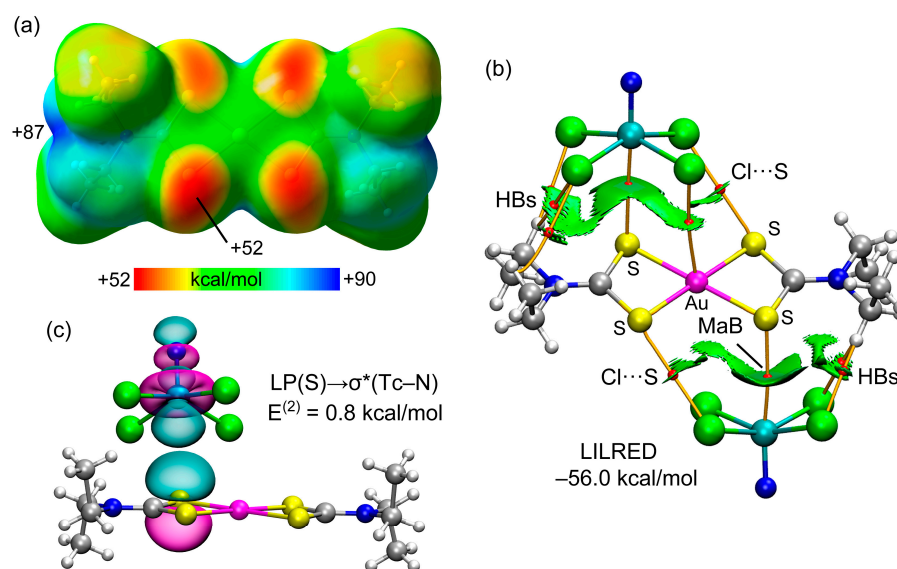


Figure 6. (a) MEP surface of cationic part *bis*(*N,N*-diethyldithiocarbamato)-gold(III) (isosurface 0.001 a.u.). Energies at selected points in kcal/mol. (b) QTAIM/NCIPlot analysis of the trimer of LILRED with indication of the interaction energy. (c) Plot of the NBOs involved in the donor–acceptor interaction of a dimer of LILRED with indication of the $E^{(2)}$ energy. Color code: Carbon grey, Chlorine green, Nitrogen blue, Technetium teal, Gold pink, Sulfur yellow, Hydrogen light grey.

3.3. Anion \cdots Lewis Base Matere Bond

Another interesting X-ray structure is shown in Figure 7 where a tetracyanonitridotechnetium(V) interacts with 4-cyanopyridine, establishing a directional Tc \cdots N MaB. In this case, a dianion $[\text{TcN}(\text{CN})_4]^{2-}$ is acting as electron acceptor [31]. In the original work, the authors considered the Tc atom as six-coordinated with the 4-cyanopyridine as an axial ligand [31]. However, the Tc \cdots N separation is longer than the sum of the covalent radii of technetium and nitrogen atoms ($\sum R_{\text{COV}} = 2.18$ Å) and the N(nitride)–Tc–C angles are approximately 100°, supporting the predominant noncovalent nature of the Tc \cdots N(py) interaction.

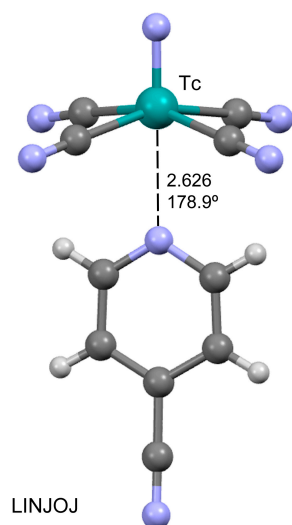


Figure 7. Ball and stick representation of the X-ray structure LINJOJ. Counter-cations omitted. Distance in Å. Color code: Carbon grey, Nitrogen blue, Technetium teal, Hydrogen light grey.

Figure 8a shows the MEP surface of the $[\text{TcN}(\text{CN})_4]^{2-}$ dianion that, as expected, exhibits large and negative MEP values in the entire surface. The existence of a σ -hole opposite to the $\text{Tc}\equiv\text{N}$ bond that corresponds to the MEP maximum (-122 kcal/mol) can be observed. The minimum is located between the CN ligands (-185 kcal/mol). The combined QTAIM/NCIplot analysis is given in Figure 8b, disclosing that the Tc and N-atoms are interconnected by a bond CP and bond path that characterize the MaB. Moreover, a dark blue RDG isosurface is coincident with the location of the bond CP, thus evidencing the attractive nature of the interaction. As also observed in SODWIR10, the blue region is flanked by yellow-reddish regions, indicating some $\text{N}\cdots\text{CN}$ repulsion. The combined QTAIM/NCIplot analysis also discloses the existence of two ancillary $\text{CH}\cdots\text{C}$ interactions characterized by bond CPs, bond paths and green RDG isosurfaces. The interaction energy is attractive (-19.7 kcal/mol) in agreement with the NCIplot analysis. The NBO analysis of the Lewis base \cdots anion dimer of LINJOJ is shown in Figure 8c, confirming the σ -hole nature of the interaction. That is, the filled LP at the sp^2 -hybridized N-atom interacts with the antibonding $\sigma^*(\text{Tc}-\text{N})$ with a concomitant stabilization energy of $E^{(2)} = 13.6$ kcal/mol, which is very significant, in line with the short $\text{Tc}\cdots\text{N}$ distance and large overlap of the donor-acceptor NBOs.

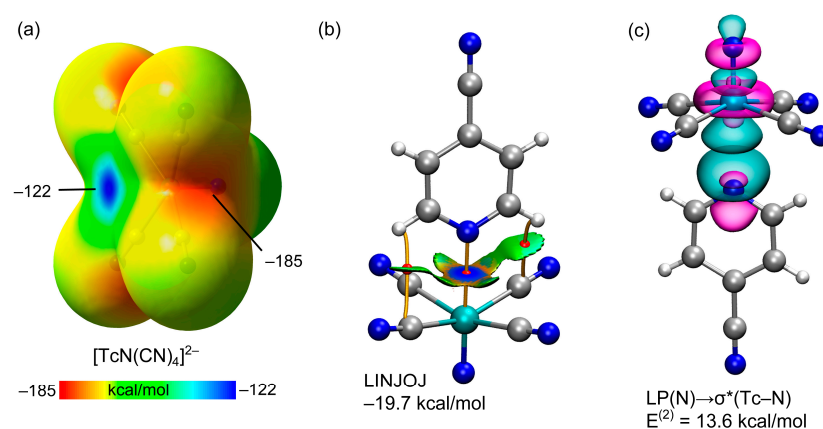


Figure 8. (a) MEP surface of $[\text{TcN}(\text{CN})_4]^{2-}$ (isosurface 0.001 a.u.). Energies at selected points in kcal/mol. (b) QTAIM/NCIplot analysis of the heterodimer of LINJOJ with indication of the dimerization energy. (c) Plot of the NBOs involved in the donor-acceptor interaction with indication of the $E^{(2)}$ energy. Color code: Carbon grey, Nitrogen blue, Technetium teal, Hydrogen light grey.

3.4. Lewis Acid ··· Lewis Base Matere Bonds

In the X-ray structures highlighted in the previous sections, the matere bond is established between an anion acting as Lewis acid and an electron rich atom belonging either to another anion, a neutral donor, or even a cation. In this section, more conventional matere bonds are described. For instance, both QUGPUE [32] and WEZNEU [33] X-ray structures form self-assembled dimers in the solid state where quite directional MaBs (see Figure 9) are established. In the case of QUGPUE, the Tc(VI) is coordinated to a tridentate ligand with an S,N,O donor set. The five-coordination of Tc(V) is completed by oxo and chlorido ligands. It can be observed in Figure 9a that the Tc(V) atom exhibits a distorted square-pyramidal coordination environment. The oxo ligand is located at the apical position and the matere bond is established opposite to this Tc=O bond, which is the most polarized. In this case, the Tc ··· S distance is 0.145 Å longer than $\Sigma R_{vdw}(Tc + S) = 3.85$ Å, thus suggesting a weaker contribution of the MaB. Remarkably, in WEZNEU, the O-atoms of the nitro groups act as electron donors and they are pointing opposite to the Te=O bonds, similarly to the MaBs observed in QUGPUE. In this case the Tc ··· O distance is well below the $\Sigma R_{vdw}(Tc + S) = 3.60$ Å. It is interesting to highlight that the nitro group is not coplanar with the imidazole ring, likely due to the formation of the MaBs.

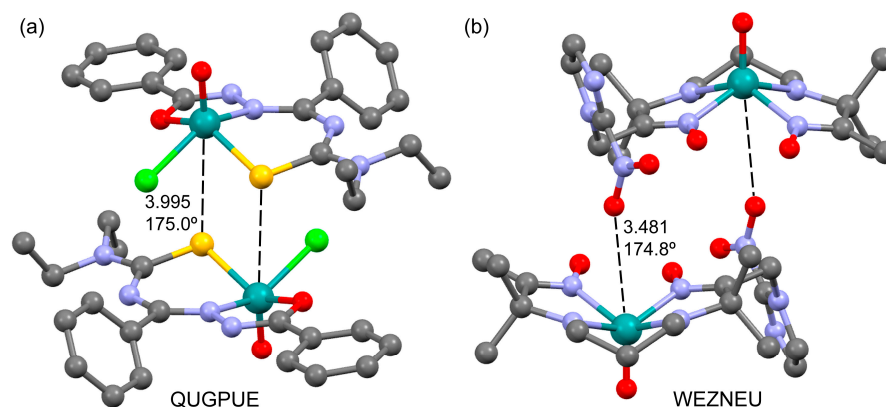


Figure 9. Ball and stick representation of the X-ray structures QUGPUE (a) and WEZNEU (b). Distances in Å. H-atoms omitted. Color code: Carbon grey, Nitrogen blue, Technetium teal, Oxygen red, Sulfur yellow.

Finally, Figure 10 shows the structure of *bis*(μ^2 -acetato)-tetrachloro-di-technetium (III) (OSICUP) [34]. The structure consists of two bridging *trans*-acetate ligands and four terminal chlorido ligands. Interestingly, this compound propagates in the solid state via four symmetrically equivalent Tc ··· Cl MaBs forming a supramolecular 1D assembly. The Tc ··· Cl distance is quite short (only 0.4 Å longer than ΣR_{cov}), thus suggesting a strong nature of these contacts as further commented below. To our knowledge, this is the first example of the matere bond for an element of group 7 with such low oxidation state and the electron donor opposite to a Tc–Tc bond.

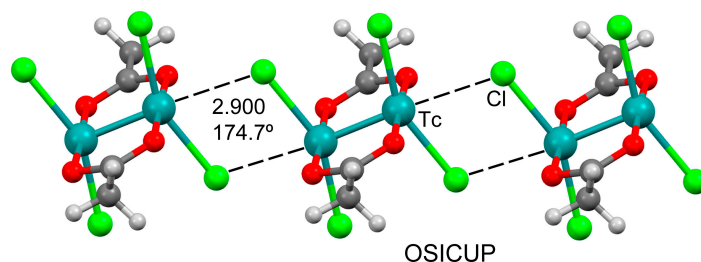


Figure 10. Ball and stick representation of the X-ray structure OSICUP. Counter-cations omitted. Distance in Å. Color code: Carbon grey, Technetium teal, Oxygen red, Hydrogen light grey.

Figure 11a shows the MEP surface of the OSICUP that discloses an intense σ -hole opposite to the Tc–Tc quadruple bond that corresponds to the MEP maximum (+31 kcal/mol). The minimum is located at the negative belt of the chlorido ligands (−19 kcal/mol). The combined QTAIM/NCIplot analysis is given in Figure 11b, evidencing that the Tc and Cl-atoms are interconnected by bond CPs and bond paths that characterize both MaBs. Moreover, two dark blue RDG isosurfaces are coincident with the location of the bond CPs, thus disclosing the attractive nature of both symmetrically equivalent Tc···Cl contacts. The blue RDG isosurfaces are connected by a long yellow-reddish region, indicating the existence of a Cl···Cl repulsion. The interaction energy is moderately strong (−11.0 kcal/mol) in line with the absence of strong electrostatic effects in this system. Each matere bond is thus estimated in −5.5 kcal/mol. The NBO analysis of the self-assembled dimer of OSICUP is shown in Figure 11c, confirming the σ -hole nature of the interaction. That is, the filled LP at the Cl-atom interacts with the antibonding σ^* (Tc–Tc) with a concomitant stabilization energy of $E^{(2)} = 13.2$ kcal/mol, which is very significant.

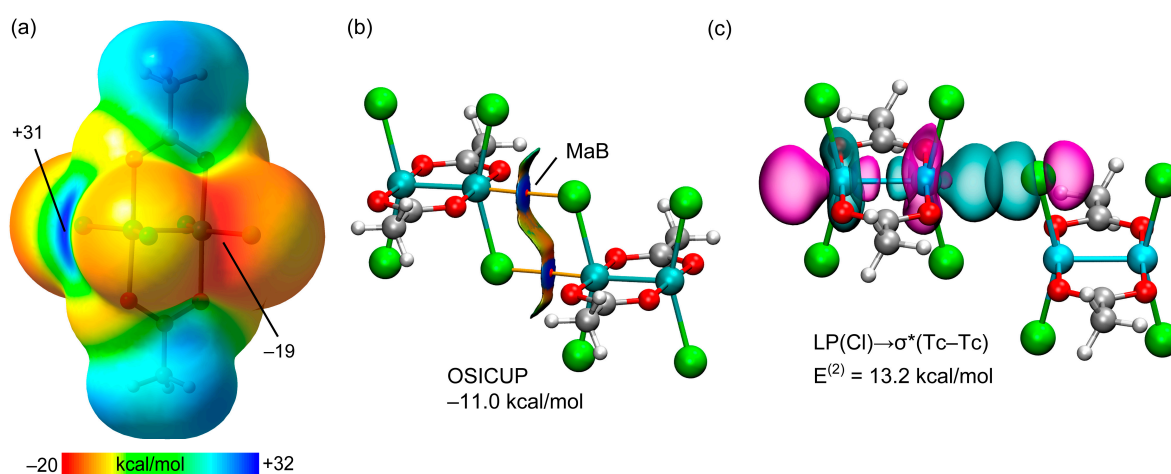


Figure 11. (a) MEP surface of OSICUP (isosurface 0.001 a.u.). Energies at selected points in kcal/mol. (b) QTAIM/NCIPlot analysis of the homodimer of OSICUP with indication of the dimerization energy. (c) Plot of the NBOs involved in the donor–acceptor interaction with indication of the $E^{(2)}$ energy. Color code: Carbon grey, Technetium teal, Oxygen red, Hydrogen light grey.

The fact that the orbital NBO contribution is larger than the binding energy agrees well with the existence of some Cl···Cl repulsion that compensates the Tc···Cl attraction. It is worthy to emphasize that this is the first example in the literature where the σ -hole interaction is opposite to a metal–metal bond.

3.5. Optimized Matere Dimers

The formation of two of the dimers described above was further analyzed by performing full geometry optimizations (Figure 12). First, the $[\text{TcNCl}_4]^- \cdots [\text{TcNCl}_4]^-$ dimer extracted from the SODWIR10 structure was computed in the gas phase and in solution. As expected, in the gas phase, the dianionic dimer is not stable and the monomers separate to infinitum. However, it should be taken into consideration that the $[\text{TcNCl}_4]^- \cdots [\text{TcNCl}_4]^-$ dimer in the solid state is under the influence of the surrounding catena-((μ^2 -18-Crown-6)-cesium counterions, which are vital for the stabilization of the $[\text{TcNCl}_4]^- \cdots ([\text{TcNCl}_4]^-)_n \cdots [\text{TcNCl}_4]^-$ polymeric chain. This effect has been partially considered by computing a dimer under the influence of the continuum solvation model and the dielectric constant (ϵ) of water. As a result, the optimization leads to a minimum with a Tc···N distance of 2.670 Å that is close to the experimental distance of 2.710 Å (Figure 12a). This result suggests that the electrostatic repulsion of the $[\text{TcNCl}_4]^- \cdots [\text{TcNCl}_4]^-$ dimer may be counterbalanced by a suitable environment and that this matere bond is possible also in solution. Unfortunately, the ϵ of any crystalline compound is unknown, however it is expected that the stabilization

of the $[\text{TcNCl}_4]^- \cdots [\text{TcNCl}_4]^-$ dimer is higher in the ionic environment of the crystalline salt than in solution. Parallel results have been reported for $[\text{AuI}_4]^- \cdots [\text{AuI}_2]^-$ dimer [3] and the $[\text{I}_3]^- \cdots [\text{I}_3]^-$ dimer [35].

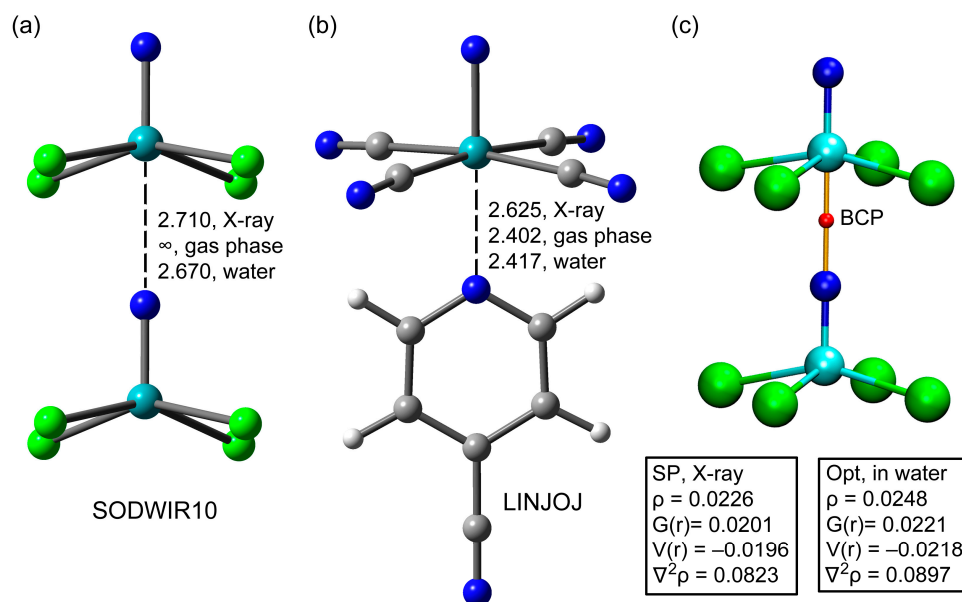


Figure 12. (a) Optimized structure of SODWIR10 in water. Distances in Å. (b) Optimized structure of LINJOJ in water. Distances in Å. (c) QTAIM analysis of the optimized dimer SODWIR10. The values of density (ρ), Lagrangian kinetic energy density $G(r)$, Potential energy density $V(r)$, and the Laplacian of the electron density $\nabla^2\rho$ are given in atomic units for the single point (SP) of the X-ray geometry and the optimized (Opt) in water. The QTAIM parameters are in a.u.

Secondly, the MaB assembly observed in LINJOJ has been also optimized (Figure 12b) where the 4-cyanopyridine interacts with the $[\text{Tc}(\text{CN})_4]^{2-}$ anion. In this case the dimer is stable both in the gas phase and in water due to the neutrality of one of the monomers. In this case the theoretical distances are 0.2 Å shorter than the experimental one, suggesting that the DFT overestimates the interaction likely due to the larger difference between the real dielectric constant in the crystal and the one of water. The fact that the fully optimized dimers of LINJOJ and SODWIR10 are stable is important to discard the possibility that the observation of the mature bonds in the solid state of these structures is simply due to packing effects.

Finally, the QTAIM analysis of the optimized SODWIR10 dimer has been performed and compared to the X-ray one (see Figure 12c). The MaB is characterized by a bond CP and bond path interconnecting the Tc and N atoms. Satisfyingly, the QTAIM parameters measured at the bond CP using a single point of the X-ray geometry and the optimized one in water are comparable, thus validating the QTAIM analysis of the X-ray structures reported herein.

4. Conclusions

This manuscript reports crystallographic and theoretical evidence that consistently proves the mature bond interaction between technetium derivatives in oxidation states +7, +6, +5, and +3 and lone pair donor atoms belonging to anions, cations, and Lewis bases. Some of the mature bonds highlighted in this work are unprecedented σ -hole interactions, not described before in the literature. In selected crystal structures, it is illustrated how mature bonds have an important role in dictating the X-ray packing. In particular, they are relevant in the formation of 1D supramolecular assemblies in SODWIR10 and OSICUP, and self-assembled homodimers in QUGPUE and WEZNEU. In the cocrystal of 4-cyanopyridine and tetracyano-nitrido-technetium (v), a short MaB involving Tc (V) governs the formation of

heterodimers (LINJOJ). In the nitridotechnetate adducts, the presence of a σ -hole opposite to the $N\equiv Tc$ bond and the participation of the antibonding $\sigma^*(N-Tc)$ orbital have been proved, strongly supporting the σ -hole nature of the MaBs reported herein. In the OSICUP structure, the participation of the $\sigma^*(Tc-Tc)$ orbital is also evidenced, which is unprecedented in the literature. Finally, the optimized dimers of SODWIR10 and LINJOJ have been computed in the gas phase and water, obtaining similar structures and confirming the importance of the MaBs as structure-directing interactions.

Author Contributions: Conceptualization, A.B., S.B., R.M.G. and A.F.; methodology, A.B., S.B., R.M.G. and A.F.; formal analysis, A.B., S.B., R.M.G. and A.F.; investigation, A.B., S.B., R.M.G. and A.F.; writing—original draft preparation, A.F.; writing—review and editing, A.B., S.B., R.M.G. and A.F.; visualization, R.M.G. and A.F.; supervision, A.F.; project administration, A.F.; funding acquisition, A.F. All authors have read and agreed to the published version of the manuscript.

Funding: This research was funded by the “Ministerio de Ciencia e Innovación” and the “Agencia Estatal de Investigación” (MICIU/AEI) of Spain (project PID2020-115637GB-I00 FEDER funds).

Institutional Review Board Statement: Not applicable.

Informed Consent Statement: Not applicable.

Data Availability Statement: Not applicable.

Acknowledgments: We thank the Centre de Tecnologies de la Informació (CTI) at University of the Balearic Islands (UIB) for the computational facilities.

Conflicts of Interest: The authors declare no conflict of interest.

References

1. Ivanov, D.M.; Bokach, N.B.; Kukushkin, V.Y.; Frontera, A. Metal Centers as Nucleophiles: Oxymoron of Halogen Bond-Involving Crystal Engineering. *Chem. Eur. J.* **2022**, *28*, e202103173. [[PubMed](#)]
2. Blasi, D.; Nicolai, V.; Gomila, R.M.; Mercandelli, P.; Frontera, A.; Carlucci, L. Unprecedented $\{dz^2-Cu^{II}O_4\} \cdots \pi$ -hole interactions: The case of a cocrystal of a Cu (II) bis-beta-diketonate complex. *Chem. Commun.* **2022**, *58*, 9524–9527. [[CrossRef](#)] [[PubMed](#)]
3. Andreo, L.; Gomila, R.M.; Priola, E.; Giordana, A.; Pantaleone, S.; Diana, E.; Mahmoudi, G.; Frontera, A. Anion \cdots Anion $[AuI_4] \cdots [AuI_2]$ Complex Trapped in the Solid State by Tetramethylammonium Cations. *Cryst. Growth Des.* **2022**, *22*, 6539–6544. [[CrossRef](#)] [[PubMed](#)]
4. Gomila, R.M.; Bauzá, A.; Mooibroek, T.J.; Frontera, A. Spodium bonding in five coordinated Zn(II): A new player in crystal engineering? *CrystEngComm* **2021**, *23*, 3084–3093. [[CrossRef](#)]
5. Bauzá, A.; Alkorta, I.; Elguero, J.; Mooibroek, T.J.; Frontera, A. Spodium Bonds: Noncovalent Interactions Involving Group 12 Elements. *Angew. Chem. Int. Ed.* **2020**, *59*, 17482–17487. [[CrossRef](#)]
6. Biswal, H.S.; Sahu, A.K.; Frontera, A.; Bauzá, A. Spodium Bonds in Biological Systems: Expanding the Role of Zn in Protein Structure and Function. *J. Chem. Inf. Model.* **2021**, *61*, 3945–3954. [[CrossRef](#)]
7. Stenlid, J.H.; Johansson, A.J.; Brinck, T. σ -Holes and σ -lumps direct the Lewis basic and acidic interactions of noble metal nanoparticles: Introducing regium bonds. *Phys. Chem. Chem. Phys.* **2018**, *20*, 2676–2692. [[CrossRef](#)]
8. Stenlid, J.H.; Brinck, T. Extending the σ -Hole Concept to Metals: An Electrostatic Interpretation of the Effects of Nanostructure in Gold and Platinum Catalysis. *J. Am. Chem. Soc.* **2017**, *139*, 11012–11015. [[CrossRef](#)]
9. Legon, A.C.; Walker, N.R. What’s in a name? ‘Coinage-metal’ non-covalent bonds and their definition. *Phys. Chem. Chem. Phys.* **2018**, *20*, 19332–19338. [[CrossRef](#)]
10. Daolio, A.; Pizzi, A.; Calabrese, M.; Terraneo, G.; Bordignon, S.; Frontera, A.; Resnati, G. Molecular Electrostatic Potential and Noncovalent Interactions in Derivatives of Group 8 Elements. *Angew. Chem. Int. Ed.* **2021**, *60*, 20723–20727. [[CrossRef](#)]
11. Daolio, A.; Pizzi, A.; Terraneo, G.; Frontera, A.; Resnati, G. Anion \cdots Anion Interactions Involving σ -Holes of Perrhenate, Pertechnetate and Permanganate Anions. *ChemPhysChem* **2021**, *22*, 2281–2285. [[CrossRef](#)] [[PubMed](#)]
12. Bauzá, A.; Frontera, A. Noncovalent Interactions Involving Group 6 in Biological Systems: The Case of Molybdopterin and Tungstopterin Cofactors. *Chem. Eur. J.* **2022**, *28*, e202201660. [[CrossRef](#)] [[PubMed](#)]
13. Calabrese, M.; Pizzi, A.; Daolio, A.; Frontera, A.; Resnati, G. σ -Hole interactions in organometallic catalysts: The case of methyltrioxorhenium(VII). *Dalton Trans.* **2023**, *52*. [[CrossRef](#)]
14. Gomila, R.M.; Frontera, A. Matere Bonds vs. Multivalent Halogen and Chalcogen Bonds: Three Case Studies. *Molecules* **2022**, *27*, 6597. [[CrossRef](#)]
15. Groom, C.R.; Bruno, I.J.; Lightfoot, M.P.; Ward, S.C. The Cambridge Structural Database. *Acta Cryst.* **2016**, *72*, 171–179. [[CrossRef](#)] [[PubMed](#)]

16. Ahlrichs, R.; Bar, M.; Haser, M.; Horn, H.; Kolmel, C. Electronic structure calculations on workstation computers: The program system turbomole. *Chem. Phys. Lett.* **1989**, *162*, 165–169. [[CrossRef](#)]
17. Grimme, S.; Antony, J.; Ehrlich, S.; Krieg, H. A consistent and accurate ab initio parametrization of density functional dispersion correction (DFT-D) for the 94 elements H-Pu. *J. Chem. Phys.* **2010**, *132*, 154104. [[CrossRef](#)]
18. Weigend, F.; Ahlrichs, R. Balanced basis sets of split valence, triple zeta valence and quadruple zeta valence quality for H to Rn: Design and assessment of accuracy. *Phys. Chem. Chem. Phys.* **2005**, *7*, 3297–3305. [[CrossRef](#)]
19. Weigend, F. Accurate Coulomb-fitting basis sets for H to Rn. *Phys. Chem. Chem. Phys.* **2006**, *8*, 1057–1065. [[CrossRef](#)]
20. Bader, R.F.W. A Quantum Theory of Molecular Structure and its Applications. *Chem. Rev.* **1991**, *91*, 893–928. [[CrossRef](#)]
21. Contreras-García, J.; Johnson, E.R.; Keinan, S.; Chaudret, R.; Piquemal, J.-P.; Beratan, D.N.; Yang, W. NCIPLOT: A program for plotting non-covalent interaction regions. *J. Chem. Theory Comput.* **2011**, *7*, 625–632. [[CrossRef](#)] [[PubMed](#)]
22. Humphrey, W.; Dalke, A.; Schulten, K. VMD: Visual molecular dynamics. *J. Mol. Graph.* **1996**, *14*, 33–38. [[CrossRef](#)] [[PubMed](#)]
23. Glendening, E.D.; Landis, C.R.; Weinhold, F. Natural Bond Orbital Methods. *WIREs Comput. Mol. Sci.* **2012**, *2*, 1–42. [[CrossRef](#)]
24. Glendening, E.D.; Badenhoop, J.K.; Reed, A.E.; Carpenter, J.E.; Bohmann, J.A.; Morales, C.M.; Karafiloglou, P.; Landis, C.R.; Weinhold, F. *NBO 7.0*; Theoretical Chemistry Institute, University of Wisconsin: Madison, WI, USA, 2018.
25. Leibnitz, P.; Reck, G.; Pietzsch, H.-J.; Spies, H. Structures of technetium and rhenium complexes. *Forschungszent. Rossendorf.* **2001**, *311*, 34.
26. Maruk, A.Y.; Grigor'ev, M.S.; German, K.E. Synthesis and crystal structure of anilinium pertechnetate and perrhenate at low and room temperatures. *Koordinatsionnaia. Khimiia.* **2010**, *36*, 381.
27. Baldas, J.; Boas, J.F.; Colmanet, S.F.; Rae, A.D.; Williams, G.A. Preparation and ESR studies of salts of crown ether complexations and nitridotechnetium(VI) anions: Structures of the twinned 'infinite sandwich' [Cs(18-crown-6)][TcNCl₄] complex and of [Rb(15-crown-5)]₂[TcNCl₄(OH₂)]. *Proceed. Royal Soc. Lond. Ser. A* **1993**, *442*, 437.
28. Gomila, R.M.; Frontera, A. Crystallographic and Theoretical Study of Osme Bonds in Nitrido-Osmium(VI) Complexes. *Inorganics* **2022**, *10*, 133. [[CrossRef](#)]
29. Bauza, A.; Mooibroek, T.J.; Frontera, A. The bright future of unconventional σ/π -hole interactions. *ChemPhysChem* **2015**, *16*, 2496–2517. [[CrossRef](#)] [[PubMed](#)]
30. Abram, U. [Au(Et₂dtc)₂][TcNCl₄]—Darstellung und Struktur. *ZAAC* **2000**, *629*, 619–620. [[CrossRef](#)]
31. Ikeda, H.; Ito, A.; Sakuda, E.; Kitamura, N.; Takayama, T.; Sekine, T.; Shinohara, A.; Yoshimura, T. Excited-State Characteristics of Tetracyanonitridorhenium(V) and -technetium(V) Complexes with N-Heteroaromatic Ligands. *Inorg. Chem.* **2013**, *52*, 6319. [[CrossRef](#)]
32. Nguyen, H.H.; Abram, U. Rhenium and technetium complexes with tridentate S,N,O ligands derived from benzoylhydrazine. *Polyhedron* **2009**, *28*, 3945–3952. [[CrossRef](#)]
33. Linder, K.E.; Chan, Y.-W.; Cyr, J.E.; Malley, M.F.; Nowotnik, D.P.; Nunn, A.D. TcO(PnAO-1-(2-nitroimidazole)) [BMS-181321], a new technetium-containing nitroimidazole complex for imaging hypoxia: Synthesis, characterization, and xanthine oxidase-catalyzed reduction. *J. Med. Chem.* **1994**, *37*, 9–17. [[CrossRef](#)] [[PubMed](#)]
34. Poineau, F.; Johnstone, E.V.; Weck, P.F.; Kim, E.; Forster, P.M.; Scott, B.L.; Sattelberger, A.P.; Czerwinski, K.R. Synthesis and Structure of Technetium Trichloride. *J. Am. Chem. Soc.* **2010**, *132*, 15864–15865. [[CrossRef](#)] [[PubMed](#)]
35. Groenewald, F.; Esterhuysen, C.; Dillen, J. Electrostatic surface potential analysis of the ion in the gas phase, the condensed phase and a novel extrapolation to the solid state. *Comput. Theor. Chem.* **2016**, *1090*, 225–233. [[CrossRef](#)]

Disclaimer/Publisher's Note: The statements, opinions and data contained in all publications are solely those of the individual author(s) and contributor(s) and not of MDPI and/or the editor(s). MDPI and/or the editor(s) disclaim responsibility for any injury to people or property resulting from any ideas, methods, instructions or products referred to in the content.